Integrated optical temporal Fourier transformer based on a chirped Bragg grating waveguide

Ksenia Dolgaleva,[1,*] Antonio Malacarne,[2] Pamela Tannouri,[2] Luís A. Fernandes,[1,3] Jason R. Grenier,[1] J. Stewart Aitchison,[1] José Azaña,[2] Roberto Morandotti,[2] Peter R. Herman,[1] and Paulo V. S. Marques[3]

[1]*Department of Electrical and Computer Engineering, University of Toronto, 10 King's College Road, Toronto, Ontario M5S 3G4, Canada*

[2]*Institut National de la Recherche Scientifique, 1650, Boulevard Lionel-Boulet, Varennes, Quebec J3X 1S2, Canada*

[3]*Instituto de Engenharia de Sistemas e Computadores do Porto (INESC-Porto), Departamento de Física e Astronomia da Universidade do Porto, Rua do Campo Alegre 687, 4169-007 Porto, Portugal*

**Corresponding author: ksenia.dolgaleva@utoronto.ca*

Received July 15, 2011; revised October 11, 2011; accepted October 12, 2011; posted October 14, 2011 (Doc. ID 150933); published November 15, 2011

We experimentally demonstrate the first integrated temporal Fourier transformer based on a linearly chirped Bragg grating waveguide written in silica glass with a femtosecond laser. The operation is based on mapping the energy spectrum of the input optical signal to the output temporal waveform by making use of first-order chromatic dispersion. The device operates in reflection, has a bandwidth of 10 nm, and can be used for incident temporal waveforms as long as 20 ps. Experimental results, obtained through both temporal oscilloscope traces and Fourier transform spectral interferometry, display a successful Fourier transformation of in-phase and out-of-phase pairs of input optical pulses, and demonstrate the correct functionality of the device for both amplitude and phase of the temporal output.

OCIS codes: 230.3120, 230.1480, 070.7145.

There exists a well-known analogy between paraxial (Fresnel) diffraction of monochromatic optical beams and narrowband dispersion of optical pulses [1]. The two phenomena can be described by mathematically identical equations, which suggests that every spatial effect has its temporal counterpart. Here we deal with an example of space-time duality, the temporal Fourier transformation by first-order chromatic dispersion, which is the temporal counterpart of the Fraunhofer free-space diffraction. By temporal (or real-time) Fourier transform, we understand the mapping of the energy spectrum of the input optical pulse (signal under test) to the time axis, i.e., frequency-to-time mapping. Real-time Fourier transformation induced by linear dispersion has been recently employed for many applications, such as real-time optical spectrum measurements [2,3], temporal magnification of broadband waveforms [4], high-frequency arbitrary microwave waveform generation [5], real-time spectroscopy [6], complex-field characterization of low intensity ultrafast optical waveforms [7], and programmable optical pulse shapers with ultrahigh update rates [8].

It has been theoretically demonstrated [3] and experimentally verified [9] that a linearly chirped fiber Bragg grating operating in reflection is capable of performing a temporal Fourier transform of an incident optical pulse, if it has a sufficient amount of first-order chromatic dispersion and a bandwidth larger than that of the incident signal. In this Letter, we report, to the best of our knowledge, the first experimental realization of an integrated optical temporal Fourier transformer (TFT). The device is based on a linearly chirped Bragg grating waveguide (LCBGW) written in silica glass with a femtosecond laser [10]. The spectral response of a linearly chirped Bragg grating (LCBG) over its reflectivity bandwidth can be expressed as $H(\omega) = |H(\omega)| \exp[\mathrm{i}(\ddot{\Phi}/2)\omega^2]$, and its corresponding temporal impulse response can be represented as $h(t) \propto \exp[\mathrm{i}\pi/(2\ddot{\Phi})t^2]$, which is mathematically identical to the amplitude response of a free-space propagation system under Fresnel conditions [3]. The grating reflectivity is given by $R(\omega) = |H(\omega)|^2$, and the first-order dispersion coefficient is the second derivative of the phase with respect to the angular frequency, $\ddot{\Phi} = -\partial^2\Phi/\partial\omega^2 = \partial\tau_g/\partial\omega$, where τ_g is the group delay. Here we are going to use the definition $\ddot{\Phi}_\lambda = \partial\tau_g/\partial\lambda = (2\pi c/\lambda_0^2)\ddot{\Phi}$, where λ_0 is the vacuum wavelength corresponding to the center of the reflectance bandgap. A LCBG can perform a temporal Fourier transform of an optical signal, extending over a time duration Δt_0, if it has a sufficient amount of dispersion, such that $|\ddot{\Phi}| \gg \Delta t_0^2/2\pi$, which is generally referred to as the temporal Fraunhofer condition [3]. It is possible to achieve a larger dispersion either by increasing the length of the grating L or by reducing the reflectivity bandwidth $\Delta\omega$, as these quantities are related by $L = c/(2n_{\mathrm{eff}})\ddot{\Phi}\Delta\omega$, where n_{eff} is the effective index of the mode in the grating. The spectral bandwidth of the optical signal under test should also be limited to $\Delta\omega$.

The LCBGWs were laser written in fused silica glass using an externally modulated femtosecond laser [10]. The laser produced frequency-doubled 300 fs, 522 nm pulses at the repetition rate of 500 kHz. An acousto-optic modulator (AOM) formed the laser burst trains with an average frequency of 500 Hz to produce a periodic refractive index modulation in the waveguides. The laser radiation was focused by an aspheric lens (40×, 0.55 NA) to a spot with the diameter of 1.6 μm (at $1/e^2$ intensity) at the depth of 75 μm below the surface of the fused silica substrate. A precision air-bearing motion stage was used

to translate the fused silica substrate with respect to the laser beam. The ratio between the speed of the translation and the AOM frequency dictated the period of the resulting Bragg grating. To produce a linear chirp in the gratings, the AOM frequency was tuned linearly, which resulted in the grating period variation 3.50 ± 0.07 nm. The speed of the sample translation was kept constant. The resulting grating waveguides are compatible with an optical fiber: they have a mode diameter of 11 μm and mode shape similar to that of a single-mode fiber.

We fabricated a 5-cm-long sample containing 20 LCBGWs with reflectivity spectrum bandwidths (and maximum reflectivities) ranging between 0.2 nm (90%) for the grating without a chirp and 18 nm (10%) for the grating with the maximum chirp. The propagation and coupling losses in our LCBGW were measured to be 0.7 dB/cm and 0.05 dB/facet, respectively, amounting to the overall insertion loss of 3.6 dB. Larger bandwidths allow processing optical waveforms with broader spectra at the expense of a lower reflectivity. The device employed to demonstrate the temporal Fourier transformation had a reflectivity bandwidth of approximately 10 nm, centered at 1550.5 nm [see Fig. 1(a)]. The skewed spectra are attributed to a higher propagation loss for those wavelength components that traveled longer distances through the device. By using the transfer matrix method and accounting for the propagation loss, we simulated the reflectivity and group delay of our LCBGWs [see Figs. 1(b) and 1(c)]. The refractive index of the grating can be represented as $n(z) = n_{\text{eff}} + \eta\{n_{\text{dc}} + n_{\text{ac}}[1 + \cos\theta(z)]\}$, where $\theta(z)$ is related to the position-dependent period of the grating $\tilde{\Lambda}(z)$ according to $\tilde{\Lambda}(z) = 2\pi/(d\theta(z)/dz)$. Here $n_{\text{eff}} = 1.4452$ is the effective refractive index of the mode in the waveguide in the absence of the periodic index modulation, $n_{\text{dc}} = 1 \times 10^{-2}$ and $n_{\text{ac}} = 2.83 \times 10^{-3}$ are the dc refractive index change and the amplitude of the ac refractive index variation in the core of the LCBGWs, respectively, and $\eta = 0.06$ is the fraction of the modal power inside of the waveguide core. The simulated reflectivity spectrum and group delay are presented in Figs. 1(b) and 1(c), respectively. The linear dispersion coefficient $\ddot{\Phi}_\lambda \approx 48$ ps/nm was found from the simulated group delay.

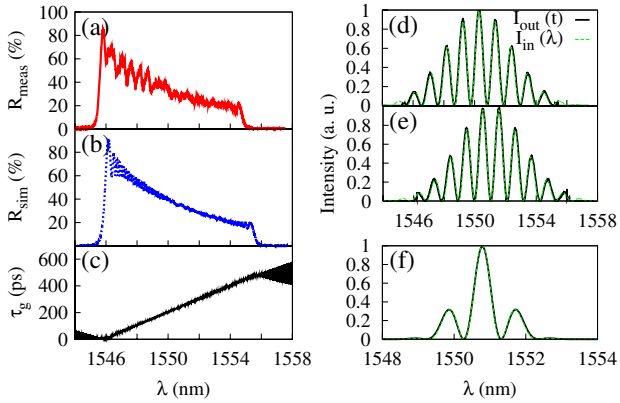

Fig. 1. (Color online) (a), (b) Reflectance spectra of the LCBGW: (a) measured (R_{meas}), (b) simulated (R_{sim}). (c) Simulated group delay of the LCBGW. (d)–(f) Simulated incident spectra (green dashed curves) and reflected temporal waveforms (black solid curves): (d), (f) for in-phase and (e) π-phase-shifted incident pulses. The simulation results shown in Figs. 1(d)–1(f) correspond to the experimental data presented in Figs. 3(a)–3(c), respectively.

To demonstrate our device operation, we used the Fourier transform spectral interferometry (FTSI) technique [11] to measure both the intensity and phase of the reflected waveform. The alternative techniques, such as frequency-resolved optical gating [12] and spectral phase interferometry for direct electrical reconstruction [13], have a disadvantage of requiring higher operating power as they are based on the nonlinear optical effects. FTSI requires postprocessing and thus does not allow performing a real-time measurement. Steps toward developing real-time single-shot techniques for optical pulse characterization are currently in progress (see, e.g., [14]).

The experimental setup used to demonstrate the temporal Fourier transform function of our LCBGW device is shown in Fig. 2. As a source of incident radiation, we used a tunable passively mode-locked fiber laser generating nearly transform-limited Gaussian pulses at a repetition rate of 16.7 MHz. The internal fiber cavity had a switchable optical bandpass filter (OBPF). In our experiment, we used Gaussian-shaped OBPFs with 3 and 5 nm bandwidths. We split the laser pulse train into two arms with a 3 dB beam splitter. In the first arm, the beam passed through a split-and-delay stage in fiber to produce the input signal under test, consisting of two pulses delayed by 7.6 ps with respect to each other. A slight variation of the laser pulse central wavelength allowed us to change the relative phase between the two pulses. In this way, we were able to obtain both in-phase and π-phase-shifted pairs of pulses. The light from the second arm served as a reference beam for the FTSI setup that was used to recover the temporal intensity and phase profiles of the reflected optical light. The dual light pulses passed into a bulk-optics setup through an input collimator. The signal was coupled into the LCBGW by a 10× microscopic objective, and, after amplification, was recombined with the reference beam to produce spectral interference. The temporal intensity profile of the output temporal waveform was captured using a fast sampling oscilloscope with a 12 ps rise-time photodiode. The FTSI technique allowed us to reconstruct a waveform with a temporal duration of up to approximately 150 ps.

In Fig. 3, we show the experimental performance of the TFT. Figures 3(a) and 3(b) display the spectra of the incident and reflected signals, together with the scaled oscilloscope traces of the temporal reflected signals for the cases when the two incident pulses were in phase and π-phase shifted, respectively. The results shown in Figs. 3(a) and 3(b) were obtained using a 5 nm filter in

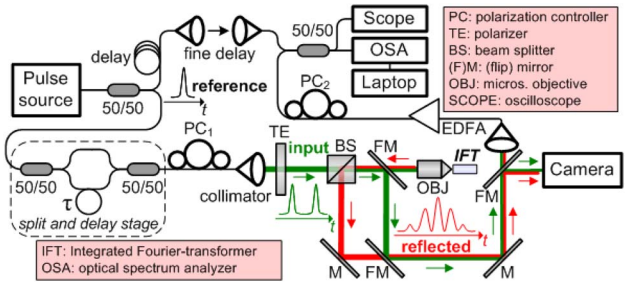

Fig. 2. (Color online) Experimental setup.

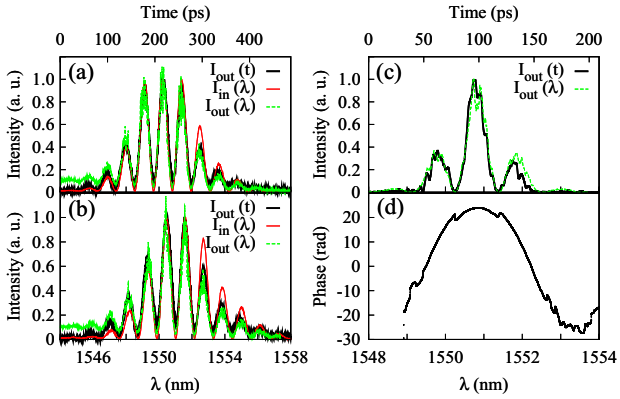

Fig. 3. (Color online) Incident (solid red curve) and reflected (dashed green curve) spectra superimposed on the scaled oscilloscope traces of the output temporal waveforms (solid black curve), obtained with a 5 nm OBPF: (a) for the in-phase incident pulses and (b) for the π-phase-shifted incident pulses. (c) Spectrum (dashed green curve) and the scaled temporal waveform (solid black curve) of the reflected in-phase double-pulse signal reconstructed through FTSI, obtained with a 3 nm OBPF. (d) The phase of the reflected signal reconstructed through FTSI.

the fiber laser source cavity. The output temporal duration in this case was around 350 ps, which is too long to be acquired by FTSI, thus we limit the representation to showing the spectra and temporal waveforms only. The measured spectral bandwidths correspond to transform-limited pulses with a time duration of 700 fs (FWHM). There is a strong similarity between the output temporal waveform and the incident spectrum. In Fig. 3(c), we show the spectrum of the reflected signal together with its scaled temporal waveform trace for a pair of in-phase incident pulses, as reconstructed through FTSI for the case when the laser operated with a 3 nm filter in the cavity. The temporal pulse duration was approximately 1.2 ps, and the output temporal duration was approximately 150 ps in this case. The phase of the reflected signal reconstructed through FTSI is shown in Fig. 3(d). The phase jumps exhibited in the plot are related to π shifts corresponding to the minima of the spectrum intensity; this represents the ultimate proof that the device provides the waveform Fourier transformation both in amplitude and phase. Using the data in Fig. 3(d), we found the dispersion coefficient of the grating to be $\ddot{\Phi}_{\lambda} \approx 34.8$ ps/nm, which satisfies the temporal Fraunhofer condition for signals as long as 20 ps. This dispersion coefficient value was used for scaling the temporal waveforms in Figs. 3(a)–3(c) along the wavelength axis. We attribute the difference between the measured and simulated values of the dispersion coefficient to the fact that we did not take into account the waveguide dispersion and relied on the plane-wave approximation.

In Figs. 1(d)–1(f), we show the simulated reflected temporal waveforms superimposed on the incident spectra after a proper scaling using the simulated dispersion coefficient value. The spectra and temporal waveforms in Figs. 1(d)–1(f) correspond to the experimental measurements shown in Figs. 3(a)–3(c), respectively. The simulations and experimental data are in good agreement and present a solid evidence of the device operation as an optical TFT in the subpicosecond to picosecond ranges.

In conclusion, we have experimentally demonstrated the performance of a femtosecond laser-written LCBGW with a 10 nm bandwidth as a TFT of (sub-)picosecond optical pulses. This experiment represents a very promising first step toward the realization of ultrafast pulse processing devices.

This work was supported by a Natural Sciences and Engineering Research Council of Canada (NSERC) Strategic Project Grant, the Canadian Institute for Photonic Innovation, the Portuguese Fundação para a Ciência e Tecnologia, and a Mitacs Elevate postdoctoral fellowship.

References

1. B. H. Kolner, IEEE J. Quantum Electron. **30**, 1951 (1994).
2. Y. C. Tong, L. Y. Chan, and H. K. Tsang, Electron. Lett. **33**, 983 (1997).
3. M. A. Muriel, J. Azaña, and A. Carballar, Opt. Lett. **24**, 1 (1999).
4. F. Coppinger, A. S. Bhushan, and B. Jalali, IEEE Trans. Microwave Theory Tech. **47**, 1309 (1999).
5. J. Chou, Y. Han, and B. Jalali, IEEE Photon. Technol. Lett. **15**, 581 (2003).
6. D. R. Solli, J. Chou, and B. Jalali, Nat. Photon. **2**, 48 (2008).
7. M. H. Asghari, Y. Park, and J. Azaña, Opt. Express **18**, 16526 (2010).
8. S. Thomas, A. Malacarne, F. Fresi, L. Potí, A. Bogoni, and J. Azaña, J. Lightwave Technol. **28**, 1832 (2010).
9. J. Azaña, L. R. Chen, M. A. Muriel, and P. W. E. Smith, Electron. Lett. **35**, 2223 (1999).
10. H. Zhang and P. R. Herman, IEEE Photon. Technol. Lett. **21**, 277 (2009).
11. L. Lepetit, G. Cheriaux, and M. Joffre, J. Opt. Soc. Am. B **12**, 2467 (1995).
12. K. W. DeLong and R. Trebino, J. Opt. Soc. Am. A **11**, 2429 (1994).
13. C. Iaconis and I. Walmsley, Opt. Lett. **23**, 792 (1998).
14. Y. Park, M. Scaffardi, A. Malacarne, L. Potí, and J. Azaña, Opt. Lett. **35**, 2502 (2010).